

# Individual dose assessment in $^{99m}\text{Tc}$ -GSA hepatic scintigraphy using a nine-compartment biokinetic model

K.D. Pham<sup>1,2,\*</sup>, K. Yamazaki<sup>1</sup>, R. Nishii<sup>1</sup>, K. Tani<sup>1</sup>, O. Kurihara<sup>1</sup>, K. Inoue<sup>2</sup>, M. Fukushi<sup>2</sup>, T. Higashi<sup>1</sup>

<sup>1</sup>National Institutes for Quantum and Radiological Science and Technology, 4-9-1 Anagawa, Inage-ku, Chiba-shi, Chiba 263-8555 Japan

<sup>2</sup>Tokyo Metropolitan University, 7-2-10 Higashi-Ogu, Arakawa-ku, Tokyo 116-8551 Japan

\*Corresponding author's e-mail: pham-dang-khoa@ed.tmu.ac.jp

**Abstract.** Technetium-99m-galactosyl human serum albumin ( $^{99m}\text{Tc}$ -GSA) is a molecular imaging agent used for evaluating hepatic function.  $^{99m}\text{Tc}$ -GSA hepatic scintigraphy examinations were performed in 50 patients from December 2018 to November 2019 at the QST Hospital in Japan. In order to estimate the individual variation in absorbed doses for each patient, a method of internal dose assessment for multiple organs and tissues in  $^{99m}\text{Tc}$ -GSA scintigraphy was developed using a nine-compartment biokinetic model that took advantage of the existing models. This method is also expected to give a better understanding of metabolic changes along with the disease progress. Transfer rates related to the liver and blood compartments of the biokinetic model were optimized for each examination by comparing the time-activity curves for the liver and heart derived from the model with those clinically observed on individual dynamic images over the trunk region using the gamma camera after intravenous injection of  $^{99m}\text{Tc}$ -GSA. Simultaneous differential equations describing the activity in each compartment were numerically analyzed using EQUATRAN-G, a commercial software, by that the total amount of disintegrations taken place in each compartment over a period of 2.5 days, which corresponds to nearly 10 physical half-lives of  $^{99m}\text{Tc}$ , was obtained. Absorbed doses of several organs and tissues were calculated using the internal dose calculation software, IDAC-Dose 2.1. As a result, the calculated average dose per unit administered activity (mGy/MBq) for the liver was the highest ( $0.058 \pm 0.007$  mGy/MBq for females and  $0.042 \pm 0.009$  mGy/MBq for males) compared to other organs and tissues, and the average dose for males was lower than that estimated for healthy males in a past study (0.054 mGy/MBq).

**KEYWORDS:**  $^{99m}\text{Tc}$ -GSA; hepatic scintigraphy; internal dose assessment; biokinetic model.

## 1 INTRODUCTION

Nuclear medicine examinations have been performed for decades in many countries by introducing specific radiopharmaceuticals into the human body. Although radiopharmaceuticals are useful for providing essential diagnostic information about their distribution in certain organs, appropriate management of medical exposure to these biomolecular agents is required to minimize their potential risk. For this purpose, the International Commission on Radiological Protection (ICRP) has provided estimations of absorbed dose per unit administered activity for various radiopharmaceuticals for the reference person through its publications [1-6]. Recently, the diagnostic reference levels (DRLs), which was introduced by the ICRP as an effective tool that aids in optimization of protection in the medical exposure [7], has been periodically established and reported by multiple countries for nuclear medicine examinations [8, 9]. A method of internal dose assessment for individual patients considering their physical and biological characteristics needs to be developed to further improve medical exposure management in nuclear medicine.

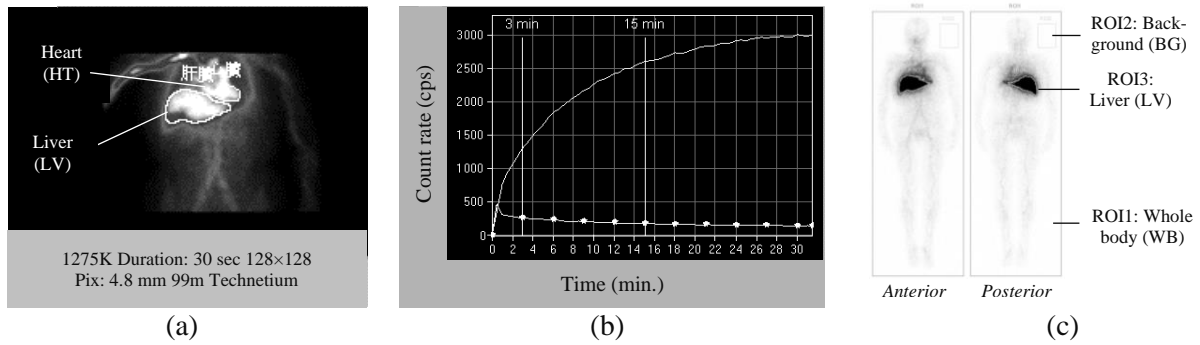
Technetium-99m galactosyl-human-serum-albumin ( $^{99m}\text{Tc}$ -GSA) is a labeled-radionuclide particularly binds to asialoglyco-protein receptor (ASGPR), which can be found with abundance in hepatocytes. Since ASGPR tends to be reduced in accordance with hepatic abnormalities and  $^{99m}\text{Tc}$ -GSA accumulation in the liver correspondingly reflects the functioning hepatic mass [10], this radiopharmaceutical is widely used for evaluation of liver function, mostly in clinical practice in Japan and preclinical practice - which was conducted on animals for research purposes - in other countries [11-15]. However, biokinetic model and absorbed dose for  $^{99m}\text{Tc}$ -GSA scintigraphy have not yet been presented in the aforementioned ICRP publications. The present study performed internal dose assessments for the patients who received  $^{99m}\text{Tc}$ -GSA hepatic scintigraphy at QST Hospital in Japan and investigated individual differences in the organ and tissue doses. In order to estimate the individual absorbed doses for each patient, a method of internal dose assessment in  $^{99m}\text{Tc}$ -GSA hepatic scintigraphy was developed using a nine-compartment biokinetic model, which took advantage of the existing models [16-18].

## 2 MATERIALS AND METHODS

### 2.1 Study Subjects, Imaging Protocol and Clinical Data Analysis

This study was approved by the ethics committee at the National Institutes for Quantum and Radiological Science and Technology – National Institute of Radiological Sciences (QST-NIRS) (approval number: 19-027). Fifty patients (18 females and 32 males) with liver tumor were recruited for this study and underwent  $^{99m}\text{Tc}$ -GSA hepatic scintigraphy from December 2018 to November 2019 at QST Hospital in Japan before receiving heavy-ion radiation therapy. Eleven of these 50 patients additionally underwent the same examination after the heavy-ion radiation therapy, and so the results from a total of 61  $^{99m}\text{Tc}$ -GSA examinations are included in this study. The ages of these patients ranged from 41 to 88 years old, with an average age of 70.8 years old. The administered activity for the respective group of patients ranged from 152.3 to 305.9 MBq, with an average value of 219.6 MBq. After receiving the injection, the patients underwent a dynamic imaging protocol in the supine position using the gamma camera, Siemens E.cam Signature Series with low-medium energy general purpose collimator, located over the trunk region, as shown in Fig. 1 (a). Digital images with a matrix of  $128 \times 128$  pixels were continuously obtained using a 30-second/frame interval, thus forming a series of 63 frames that covered a duration of 31.5 minutes. The time-activity curves, which were expressed in terms of count rate (counts per second [cps]), were plotted for the regions of interest (ROIs) of the heart and liver in each frame, as shown in Fig. 1 (b). Whole-body scanning was performed immediately after the dynamic imaging protocol and the counts from the anterior and posterior gamma cameras in the ROIs of the whole body, liver, and background were recorded, as shown in Fig. 1 (c).

**Figure 1:** Imaging protocol using the gamma camera: (a) dynamic image for the trunk region; (b) time-activity curves for the ROIs of the liver and heart; (c) whole-body scanning images.



The gamma camera sensitivities for the liver ( $s_{LV}$ ) and heart ( $s_{HT}$ ) in the dynamic imaging protocol were calculated for each examination using equations (1) and (2), respectively:

$$s_{LV} = \frac{P_{LV,t}}{A_0 \times (1/2)^{\frac{t}{t_{1/2}}} \times \frac{c_{LV} - (c_{BG}/pix_{BG}) \times pix_{LV}}{c_{WB} - (c_{BG}/pix_{BG}) \times pix_{WB}}} \quad (1)$$

and

$$s_{HT} = \frac{P_{HT,t}}{A_0 \times (1/2)^{\frac{t}{t_{1/2}}} \times \frac{9/90 \left( [c_{WB} - (c_{BG}/pix_{BG}) \times pix_{WB}] - [c_{LV} - (c_{BG}/pix_{BG}) \times pix_{LV}] \right)}{c_{WB} - (c_{BG}/pix_{BG}) \times pix_{WB}}} \quad (2)$$

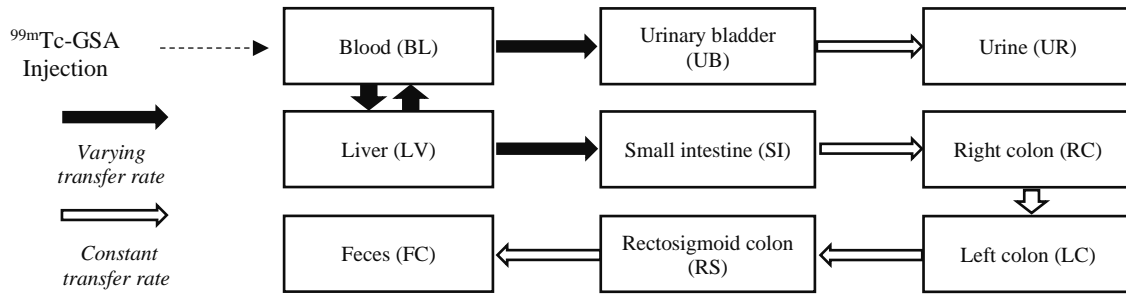
where  $A_0$  is the initial administered activity (Bq),  $t_{1/2}$  is the physical half-life of  $^{99m}\text{Tc}$  (min.),  $c_i$  is the number of counts in the ROI of  $i$ , and  $pix_i$  is the number of pixels in the ROI of  $i$ .  $c_i$  and  $pix_i$  are the average values recorded from the anterior and posterior gamma cameras during whole-body scanning. The average sensitivity of the anterior and posterior gamma cameras during whole-body scanning was

assumed to be uniform for the radionuclides in the body because count rates related to the relative positions of organs can be offset during the scanning of the patient by maintaining a constant distance from each gamma camera to the surface of the body. Besides, as observed from the whole-body image,  $^{99m}\text{Tc}$ -GSA was distributed mostly in the liver and blood. In equation (2), the number of counts from the radionuclides in the heart was calculated by assuming that 90% of the total blood volume is present in other organs and tissues except the liver and that 9% of the total blood volume is present in the heart [19].  $p_{LV,t}$  and  $p_{HT,t}$  are the count rates for the ROIs of the liver and heart in the dynamic imaging protocol. Whole-body scanning was performed immediately after the dynamic imaging protocol; hence,  $t$  should have a value of 31.5 (minutes).

## 2.2 Biokinetic Model

The sequential image acquisition for  $^{99m}\text{Tc}$ -GSA hepatic scintigraphy was basically designed to be performed within 31.5 minutes in consideration of the comfort of the patient and clinical efficiency; hence, the nine-compartment biokinetic model for  $^{99m}\text{Tc}$ -GSA, which can predict the total number of disintegrations that occur in each compartment beyond the execution period of the dynamic imaging protocol, was developed as shown in Fig. 2.

**Figure 2:** Nine-compartment biokinetic model for  $^{99m}\text{Tc}$ -GSA.



As it was intravenously injected into the patients,  $^{99m}\text{Tc}$ -GSA was expected to spread primarily into the blood stream, then scatter into the bladder or liver via two discrete secondary routes. The bladder route ended in the urine, while the liver route terminated in the feces as excretory compartments. The change in activity by time after the injection in a certain compartment  $i$  was defined by equation (3) [6]:

$$\frac{dq_i}{dt} = -\lambda_{ii}q_i(t) - \lambda_d q_i(t) + \sum_{\substack{j=1 \\ j \neq i}}^n \lambda_{ji}q_j(t) \quad (3)$$

where  $\lambda_{ii}$  is the transfer rate of substances escaping compartment  $i$  per unit time ( $\text{d}^{-1}$ ),  $\lambda_{ji}$  is the transfer rate of substances from compartment  $j$  entering compartment  $i$  per unit time ( $\text{d}^{-1}$ ),  $\lambda_d$  is the radioactive decay constant, and  $q_i(t)$  is the amount of substances in compartment  $i$ . Regarding the transfer rates in this model, four of them ( $\lambda_{BL,LV}$ ,  $\lambda_{BL,UB}$ ,  $\lambda_{LV,BL}$ ,  $\lambda_{LV,SI}$ ) were classified as varying rates that may fluctuate among individual patients, while the other rates depend on physical properties rather than chemical properties, and they were determined to be constant as shown in Table 1.

**Table 1:** Values of the transfer rates determined to be constant

Transfer rate	Constant value
$\lambda_{BL,UB}$	12 [17]
$\lambda_{SI,RC}$	6 [20]
$\lambda_{RC,LC}$	2 [20]
$\lambda_{LC,RS}$	2 [20]
$\lambda_{RS,FC}$	2 [20]

### 2.3 Curve Fitting with Eigenanalysis Method and Chi-square Test

The combination of the four varying transfer rates was optimized using the least square fitting method [21-23] by comparing the time-activity curves for the liver and heart predicted by model calculation with those that were clinically observed. In the model calculation, since the combination of four free parameters results in high complexity with a multitude of trials required to determine reasonable values for the varying transfer rates for each patient, the system of the following differential equations (4) was solved by the eigenanalysis method [24]:

$$\begin{aligned} \frac{dq_{BL}}{dt} &= \lambda_{LV,BL} \times q_{LV} - (\lambda_{BL,LV} + \lambda_{BL,UB} + \lambda_{Tc-99m}) \times q_{BL} \\ \frac{dq_{LV}}{dt} &= \lambda_{BL,LV} \times q_{BL} - (\lambda_{LV,BL} + \lambda_{LV,SI} + \lambda_{Tc-99m}) \times q_{LV} \end{aligned} \quad (4)$$

Principally, the system of equations (4) is a type of first-order differential equation and can be written in a general form as shown in equation (5):

$$\begin{aligned} y_1' &= k_1 y_1 + k_2 y_2 \\ y_2' &= k_3 y_1 + k_4 y_2 \end{aligned} \quad \left( P = \begin{bmatrix} k_1 & k_2 \\ k_3 & k_4 \end{bmatrix} \right) \quad (5)$$

The exact solutions  $y_1(t)$  and  $y_2(t)$  are shown in equation (6):

$$\begin{aligned} y_1(t) &= \frac{-[(k_1 - \lambda_2)e^{\lambda_1 t} - (k_1 - \lambda_1)e^{\lambda_2 t}]y_1(0) - k_2(e^{\lambda_1 t} - e^{\lambda_2 t})y_2(0)}{\lambda_2 - \lambda_1} \\ y_2(t) &= \frac{(k_1 - \lambda_1)(k_1 - \lambda_2)(e^{\lambda_1 t} - e^{\lambda_2 t})y_1(0) + k_2[(k_1 - \lambda_1)e^{\lambda_1 t} - (k_1 - \lambda_2)e^{\lambda_2 t}]y_2(0)}{k_2(\lambda_2 - \lambda_1)} \end{aligned} \quad (6)$$

where  $\lambda_1$  and  $\lambda_2$  are the eigenvalues of matrix  $P$  given in equation (5), and  $y_1(0)$  and  $y_2(0)$  are the initial values of the variables  $y_1$  and  $y_2$ . In this study, the initial values of all organs and tissues were designated as 0 (zero), except for that of blood, which was set based on the initial administered activity (Bq).

For the comparison between the model calculation and clinical data, the gamma camera sensitivities calculated using equations (1) and (2) were applied to the activity obtained by the model. Also, the chi-square test [25] using equation (7) was applied to assess the goodness of fit:

$$\chi_0^2 = \sum_{i=1}^n \left( \frac{\ln(O_i) - \ln(E_i)}{\ln(SF)} \right)^2 \quad (7)$$

where  $\chi_0^2$  is the chi-square value,  $O_i$  is the clinically observed count rate during frame  $i$  in the dynamic imaging protocol,  $E_i$  is the calculated count rate during frame  $i$ , and  $SF$  is the scattering factor. A value of 1.2 was assigned for  $SF$  as a typical value in *in vivo* measurements for radionuclides that emit high energy photon (>100 keV) [25]. The  $p$ -value which represents the chances of obtaining a higher  $\chi^2$  value than  $\chi_0^2$  was evaluated with  $n-1$  degrees of freedom, and the results were considered unfit and rejected if the  $p$ -value was 5% or less.

### 2.4 Dose Calculation

According to ICRP Publication 128 [6], absorbed dose is calculated using the following equation (8):

$$D_{(T \leftarrow S)} = \tilde{A}_S \times S_{(T \leftarrow S)} \quad (8)$$

where  $D_{(T \leftarrow S)}$  is the absorbed dose from source organ  $S$  to target organ  $T$  (mGy),  $\tilde{A}_s$  is the cumulated activity (MBq·hour), and  $S_{(T \leftarrow S)}$  is the absorbed dose in target organ  $T$  per unit activity in source organ  $S$  (mGy/MBq·hour).  $S_{(T \leftarrow S)}$  is calculated for each radionuclide based on the database of specific absorbed fractions (SAF) provided in ICRP Publ. 133 [26], and  $\tilde{A}_s$  is the main variable to be computed as it differs among patients. The varying transfer rates determined by least square fitting method were used to complete the full specification of the nine-compartment biokinetic model, and  $\tilde{A}_s$  value of each compartment over 2.5 days, which is equivalent to 10 physical half-lives of  $^{99m}\text{Tc}$ , was obtained using EQUATRAN-G (Omega Simulation, Tokyo, Japan), which is a commercial software specializing in numerical analysis. This parameter was used as an input for IDAC-Dose 2.1 [27], an internal dose calculation software, to assess the absorbed doses for organs and tissues.

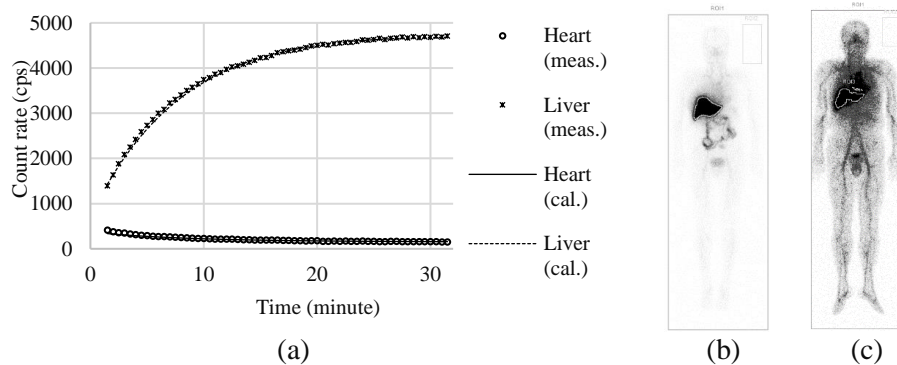
### 3 RESULTS AND DISCUSSION

#### 3.1 Sensitivity of the Gamma Camera and Curve Fitting

The gamma camera sensitivities in the dynamic imaging protocol were evaluated to be  $4.2 \times 10^{-5} \pm 7.2 \times 10^{-6}$  cps/Bq and  $2.9 \times 10^{-5} \pm 1.6 \times 10^{-5}$  cps/Bq for the ROIs of the liver and heart on average among the examinations, respectively. These results imply that each individual had a unique absorption rate in the body, and the distance between the surfaces of the gamma cameras and the body varied among patients. The liver was generally aligned at the center of the field-of-view while the heart was located closer to the top edge. Nevertheless, the average sensitivities are comparable with each other in terms of magnitude because the sensitivity of the gamma camera with an appropriate collimator was maintained to be uniform within the field-of-view.

In this study, four varying transfer rates were optimized for 61  $^{99m}\text{Tc}$ -GSA examinations, of which 55 cases were found to be acceptable in terms of goodness of fit using the chi-square test. Meanwhile, several exceptional cases (6 cases) were ultimately excluded from the study based on their whole-body scanning information, which had disagreement with the description of the nine-compartment model. In these cases,  $^{99m}\text{Tc}$ -GSA had already distributed in certain organs and tissues other than the liver and blood within the first 31.5 minutes after the injection. Typical results of the time-activity curves and whole-body scanning of cases with acceptable goodness of fit are presented in Fig. 3 (a) and (b), respectively, while the whole-body scanning of a typical excluded case is shown in Fig. 3 (c).

**Figure 3:** (a) Time-activity curves predicted by the model (cal.) compared with clinical measurements (meas.); (b) whole-body scanning with anterior gamma camera of an acceptable case; (c) whole-body scanning with anterior gamma camera of excluded case.

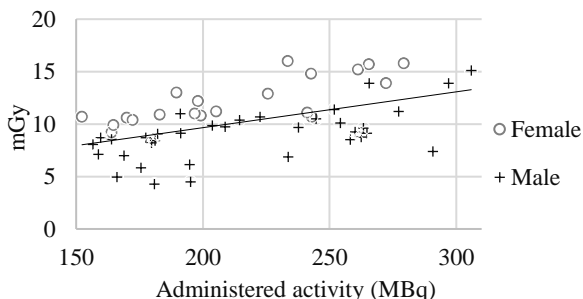


Cases with acceptable goodness of fit usually had a decent  $^{99m}\text{Tc}$ -GSA concentration in the liver as what it was designated for. Remarkably, every excluded case had abnormal distribution of  $^{99m}\text{Tc}$ -GSA, and the radionuclides were diffused throughout the adjacent organs. Four patients involved in six excluded cases (two patients took the examination twice) were confirmed to have extremely poor liver function. Although the model developed in this study was applicable to most of the patients with liver tumor, it was not applicable to exceptional cases similar to that shown in Fig. 3 (c). Thus, further study is needed to improve the model so that it can be applied even in patients with extremely poor hepatic function.

### 3.2 Individual Absorbed Dose

Absorbed doses in 55 cases with acceptable goodness of fit were calculated, and the average dose to the liver ( $0.048 \pm 0.011$  mGy) was estimated to be the highest among all organs and tissues. As shown in Fig. 4, although the liver dose had a vague tendency to be higher when the administered activity increased, it was substantially dependent on individual biokinetics.

**Figure 4:** Study population statistics: Absorbed dose to the liver.



Absorbed doses per unit administered activity in several organs and tissues are presented in Table 2. Since  $^{99m}\text{Tc}$ -GSA is mostly concentrated in the liver, this organ received the highest absorbed dose per unit administered activity, while the gallbladder ranked second. It is possible that the adjacent position of the gallbladder to the liver accounts for that result. Female patients tend to receive higher doses in various organs than male patients, especially in the liver and gallbladder. It was suggested that this occurs [27] because the female and male phantoms used for the dose calculation in accordance with ICRP Publication 110 [28] were different in terms of the mass of the liver (1.4 kg for females; 1.8 kg for males) and blood (0.856 kg for females; 1.032 kg for males).

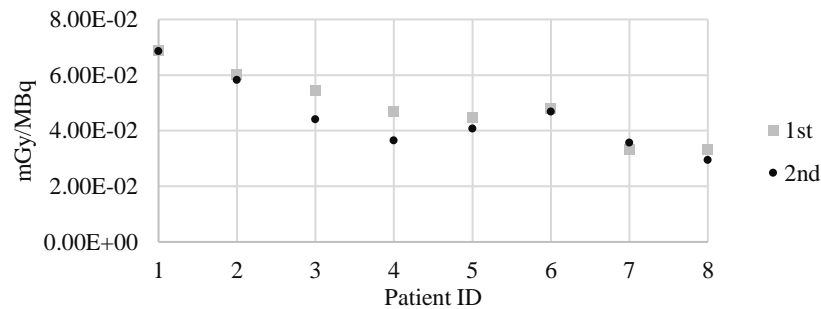
**Table 2:** Absorbed dose per unit administered activity (mGy/MBq) estimated in this study and estimated for healthy male volunteers in the reference study.

Organ dose (mGy/MBq)	Females (20 cases)	Males (35 cases)	Reference [29]
Colon wall	$6.2 \times 10^{-3} \pm 9.6 \times 10^{-4}$	$1.0 \times 10^{-2} \pm 5.5 \times 10^{-3}$	$7.9 \times 10^{-2}$
Gallbladder wall	$3.1 \times 10^{-2} \pm 3.9 \times 10^{-3}$	$2.7 \times 10^{-2} \pm 4.3 \times 10^{-3}$	$6.5 \times 10^{-2}$
Kidneys	$1.6 \times 10^{-2} \pm 6.9 \times 10^{-4}$	$1.2 \times 10^{-2} \pm 1.4 \times 10^{-3}$	$8.1 \times 10^{-3}$
Liver	$5.8 \times 10^{-2} \pm 6.5 \times 10^{-3}$	$4.2 \times 10^{-2} \pm 9.1 \times 10^{-3}$	$5.4 \times 10^{-2}$
Ovaries	$4.9 \times 10^{-3} \pm 7.1 \times 10^{-4}$	-	$1.0 \times 10^{-2}$
Red bone marrow	$1.5 \times 10^{-2} \pm 9.8 \times 10^{-4}$	$8.5 \times 10^{-3} \pm 1.4 \times 10^{-3}$	$5.4 \times 10^{-3}$
Small intestine wall	$8.5 \times 10^{-3} \pm 5.2 \times 10^{-4}$	$8.2 \times 10^{-3} \pm 3.2 \times 10^{-3}$	$2.6 \times 10^{-2}$
Testes	-	$1.0 \times 10^{-3} \pm 1.9 \times 10^{-4}$	$1.1 \times 10^{-3}$
Urinary bladder wall	$1.7 \times 10^{-3} \pm 1.1 \times 10^{-3}$	$3.8 \times 10^{-3} \pm 3.3 \times 10^{-3}$	$1.5 \times 10^{-2}$

There are two possible factors accounted for the difference between our results with the reference dose: the study subjects and the method of assessment. First, the subjects in the reference study were healthy males from 23 to 30 years old, while the subjects in our study were unhealthy males and females from 41 to 88 years old (39 out of 61 subjects were older than 70). Also, the reference study was conducted based on laboratory measurements including on-site hematology analysis. Meanwhile, our study relied on clinical observation and several assumptions. Unlike the reference results, the calculated absorbed dose in the gallbladder in our study was lower than that in the liver. The reason for this is that the gallbladder was excluded from the biokinetic model due to a lack of available information, to the best of the knowledge of the author concerning the excretion rate from the liver to the gallbladder. However, in both studies, it is clear that absorbed dose in the liver was considerably high compared with the other organs and tissues. In general, the average liver dose estimated in this study for males with liver tumor ( $0.042 \pm 0.009$  mGy/MBq) was lower than the reference dose estimated for healthy males ( $0.054$  mGy/MBq) [29].

Among 11 patients who underwent  $^{99m}\text{Tc}$ -GSA twice, eight had relatively similar absorbed doses in their two examinations (Fig. 5), and two had incredibly poor liver function such that the radiopharmaceuticals spread to neighboring organs, making it impossible to fit their time-activity curves and assess the absorbed dose in both examinations. Nevertheless, there was one exceptional patient whose first examination was acceptable in terms of goodness of fit, but the her second examination was excluded due to her worsening liver condition after heavy-ion radiotherapy. In the future, the effect of liver volume should also be considered in order to perform an accurate dose assessment.

**Figure 5:** Comparison of absorbed dose per unit administered activity between two examinations



#### 4 CONCLUSION

This study developed a nine-compartment biokinetic model for  $^{99m}\text{Tc}$ -GSA examinations and performed individual dose assessment for patients with liver tumor. The model was applicable in most of the cases, but not for several exceptional cases in which a certain amount of  $^{99m}\text{Tc}$ -GSA had already been distributed in certain organs and tissues other than the liver and blood within the first 31.5 minutes after the injection. Thus, further study is needed to improve the model, so that it is applicable even for patients with extremely poor hepatic function.

Absorbed doses for the 55 cases to which the developed model was applied were calculated, and the average dose to the liver was estimated to be the highest among all of the organs and tissues, with an average value of  $0.048 \pm 0.011$  mGy. Although it had a vague tendency to be higher when the administered activity increased, the liver dose was substantially dependent on individual biokinetics. The average dose per unit administered activity for the liver was calculated to be  $0.042 \pm 0.009$  mGy/MBq for males, which was lower than that estimated for healthy males in a past study ( $0.054$  mGy/MBq).

#### 5 REFERENCES

- [1] ICRP, 1971. Protection of the Patient in Radionuclide Investigations. ICRP Publication 17. Pergamon Press, Oxford.
- [2] ICRP, 1988. Radiation Dose to Patients from Radiopharmaceuticals. ICRP Publication 53. Ann. ICRP 18 (1-4).
- [3] ICRP, 1992. Radiological Protection in Biomedical Research. ICRP Publication 62. Ann. ICRP 22 (3).
- [4] ICRP, 1998. Radiation Dose to Patients from Radiopharmaceuticals (Addendum to ICRP Publication 53). ICRP Publication 80. Ann. ICRP 28 (3).
- [5] ICRP, 2008. Radiation Dose to Patients from Radiopharmaceuticals - Addendum 3 to ICRP Publication 53. ICRP Publication 106. Ann. ICRP 38 (1-2).
- [6] ICRP, 2015. Radiation Dose to Patients from Radiopharmaceuticals: A Compendium of Current Information Related to Frequently Used Substances. ICRP Publication 128. Ann. ICRP 44(2S).
- [7] ICRP, 2017. Diagnostic reference levels in medical imaging. ICRP Publication 135. Ann. ICRP 46(1).
- [8] K. Abe, M. Hosono, T. Igarashi, et al, 2020. The 2020 national diagnostic reference levels for nuclear medicine in Japan. Ann. Nucl Med, 34, 799–806.

- [9] H. C. Song, M. H. Na, J. Kim, et al, 2019. Diagnostic Reference Levels for Adult Nuclear Medicine Imaging Established from the National Survey in Korea. *Nucl Med Mol Imaging*, 53(1), 64-70.
- [10] T. Sawamura, H. Nakada, H. Hazama, et al, 1984. Hyperasialoglycoproteinemia in patients with chronic liver diseases and/or liver cell carcinoma: Asialoglycoprotein receptor in cirrhosis and liver cell carcinoma. *J Gastroenterology*, Volume 87, Issue 6, Pages 1217-1221.
- [11] W. de Graaf, R. L. Veteläinen, K. de Bruin, et al, 2008.  $^{99m}\text{Tc}$ -GSA scintigraphy with SPECT for assessment of hepatic function and functional volume during liver regeneration in a rat model of partial hepatectomy. *J Nucl Med*, 49(1), 122-8. doi: 10.2967/jnumed.107.044255.
- [12] A. Kato, Y. Nakamoto, T. Ishimori, et al, 2018. Predictability of  $^{99m}\text{Tc}$ -Galactosyl Human Serum Albumin Scintigraphy for Posthepatectomy Liver Failure. *AJR Am J Roentgenol*, 210(1), 158-165. doi: 10.2214/AJR.17.18411.
- [13] T. Iida, S. Yagi, T. Hori, et al, 2015. Significance of  $^{99m}\text{Tc}$ -GSA liver scintigraphy in liver surgery and transplantation. *Ann Transl Med*, 3(2), 16. doi: 10.3978/j.issn.2305-5839.2015.01.07
- [14] H. Nishikawa, Y. Osaki, H. Komekado, et al, 2015. Clinical implication of the preoperative GSA index in  $^{99m}\text{Tc}$ -GSA scintigraphy in hepatitis C virus-related hepatocellular carcinoma. *Oncol Rep*, 33(3), 1071-8. doi: 10.3892/or.2014.3691.
- [15] K. Kotani, J. Kawabe, S. Higashiyama, et al, 2018. Heterogeneous liver uptake of Tc- $^{99m}$ -GSA as quantified through SPECT/CT helps to evaluate the degree of liver fibrosis: A retrospective observational study. *Medicine (Baltimore)*, 97(31), e11765.
- [16] N. Shuke, T. Aburano, K. Nakajima, et al, 1992. The utility of quantitative  $^{99m}\text{Tc}$ -GSA liver scintigraphy in the evaluation of hepatic functional reserve: comparison with  $^{99m}\text{Tc}$ -PMT and  $^{99m}\text{Tc}$ -Sn colloid. *Kaku Igaku*, 29(5), 573-84 in Japanese.
- [17] ICRP, 1994. Dose Coefficients for Intakes of Radionuclides by Workers. ICRP Publication 68. *Ann. ICRP* 24 (4).
- [18] ICRP, 2006. Human Alimentary Tract Model for Radiological Protection. ICRP Publication 100. *Ann. ICRP* 36 (1-2).
- [19] ICRP, 2002. Basic Anatomical and Physiological Data for Use in Radiological Protection Reference Values. ICRP Publication 89. *Ann. ICRP* 32 (3-4).
- [20] ICRP, 2015. Occupational Intakes of Radionuclides: Part 1. ICRP Publication 130. *Ann. ICRP* 44(2).
- [21] H. J. Motulsky, et al, 1987. Fitting Curves to Data Using Nonlinear Regression: A Practical and Nonmathematical Review. *FASEB J*, 1(5), 365-74.
- [22] H. Motulsky, A. Christopoulos, 2003. Fitting Models to Biological Data Using Linear and Nonlinear Regression: A Practical Guide to Curve Fitting, GraphPad Software Inc., San Diego CA, pp. 27-28.
- [23] G. Kemmer, S. Keller, 2010. Nonlinear least-squares data fitting in Excel spreadsheets. *Nat Protoc*, 5(2), 267-81. doi: 10.1038/nprot.2009.182.
- [24] Grant B. Gustafson. Systems of Differential Equations. Retrieve 2020-09-16 from: <http://www.math.utah.edu/~gustafso/2250systems-de.pdf>
- [25] C.M. Castellani, J.W. Marsh, C. Hurtgen, et al, 2013. IDEAS Guidelines (Version 2) for the Estimation of Committed Doses from Incorporation Monitoring Data, European Radiation Dosimetry Group, pp. 44, 55-58.
- [26] ICRP, 2016. The ICRP computational framework for internal dose assessment for reference adults: specific absorbed fractions. ICRP Publication 133. *Ann. ICRP* 45(2), 1-74.
- [27] M. Andersson, L. Johansson, K. Eckerman, et al, 2017. IDAC-Dose 2.1, an internal dosimetry program for diagnostic nuclear medicine based on the ICRP adult reference voxel phantoms. *EJNMMI Res*, 7(1), 88.
- [28] ICRP, 2009. Adult Reference Computational Phantoms. ICRP Publication 110. *Ann. ICRP* 39 (2).
- [29] K. Torizuka, S. K. Ha-Kawa, K. Ikekubo, et al, 1991. Phase I clinical study on  $^{99m}\text{Tc}$ -GSA, a new agent for functional imaging of the liver. *Kaku Igaku*, 28(11), pp. 1321-31 in Japanese.